PHYSICAL REVIEW A **92**, 012106 (2015)

Stability of a trapped-atom clock on a chip

R. Szmuk,[1] V. Dugrain,[2] W. Maineult,[1] J. Reichel,[2] and P. Rosenbusch[1,*]

[1]*LNE-SYRTE, Observatoire de Paris, PSL Research University, CNRS, Sorbonne Universités, UPMC University Paris 06, 61 Avenue de l'Observatoire, 75014 Paris, France*

[2]*Laboratoire Kastler Brossel, ENS, UPMC, CNRS, 24 Rue Lhomond, 75005 Paris, France*

(Received 26 January 2015; published 10 July 2015)

We present a compact atomic clock interrogating ultracold ^{87}Rb magnetically trapped on an atom chip. Very long coherence times sustained by spin self-rephasing allow us to interrogate the atomic transition with 85% contrast at 5-s Ramsey time. The clock exhibits a fractional frequency stability of 5.8×10^{-13} at 1 s and is likely to integrate into the 10^{-15} range in less than a day. A detailed analysis of seven noise sources explains the measured frequency stability. Fluctuations in the atom temperature (0.4 nK shot-to-shot) and in the offset magnetic field (5×10^{-6} relative fluctuations shot-to-shot) are the main noise sources together with the local oscillator, which is degraded by the 30% duty cycle. The analysis suggests technical improvements to be implemented in a future second generation setup . The results demonstrate the remarkable degree of technical control that can be reached in an atom chip experiment.

DOI: 10.1103/PhysRevA.92.012106 PACS number(s): 06.20.−f, 06.30.Ft, 67.85.−d, 37.10.Gh

I. INTRODUCTION

Atomic clocks are behind many everyday tasks and numerous fundamental science tests. Their performance has made a big leap through the discovery of laser cooling [1–3] giving one the ability to control the atom position on the millimeter scale. It has led to the development of atomic fountain clocks [4,5] which have reached a stability limited only by fundamental physics properties, i.e., quantum projection noise and Fourier-limited linewidth [6]. While these laboratory-size setups are today's primary standards, mobile applications such as telecommunication, satellite-aided navigation [7] or spacecraft navigation [8] call for smaller instruments with liter-scale volume. In this context, it is natural to consider trapped atoms. The trap overcomes gravity and thermal expansion and thereby enables further gain on the interrogation time. It makes interrogation time independent of apparatus size. Typical storage times of neutral atoms range from a few seconds to minutes [9,10]. Thus a trapped-atom clock with long interrogation times could measure energy differences in the mHz range in one single shot. Hence, if trap-induced fluctuations can be kept low, trapped atoms could not only define time with this resolution, but could also be adapted to measure other physical quantities like electromagnetic fields, accelerations or rotations with very high sensitivity. A founding step towards very long interrogation of trapped neutral atoms was made in our group through the discovery of spin self-rephasing [11] which sustains several tens of seconds coherence time [11–13]. This rivals trapped-ion clocks, the best of which has shown 65-s interrogation time and a stability of 2×10^{-14} at 1 s [14,15].

It is to be compared to compact clocks using thermal vapor and buffer gas [16–18] or laser cooled atoms [19–22]. Among these the record stability is 1.6×10^{-13} at 1 s [17]. Clocks with neutral atoms trapped in an optical lattice have reached impressive stabilities down to the 10^{-18} range [23,24] but their interrogation time is so far limited by the local oscillator. Research into making such clocks transportable is ongoing [25,26]. We describe the realization of a compact clock using neutral atoms trapped on an atom chip and analyze trap-induced fluctuations.

Our "trapped-atom clock on a chip" (TACC) employs laser cooling and evaporative cooling to reach ultracold temperatures where neutral atoms can be held in a magnetic trap. Realizing a 5-s Ramsey time, we obtain 100-mHz linewidth and 85% contrast on the hyperfine transition of ^{87}Rb. We measure the fractional frequency stability as $5.8 \times 10^{-13}\tau^{-1/2}$. It is reproduced by analyzing several noise contributions, in particular atom number, temperature, and magnetic field fluctuations. The compact setup is realized through the atom chip technology [27], which builds on the vast knowledge of microfabrication. The use of atom chips is also widespread for the study of Bose-Einstein condensates [9,28], degenerate Fermi gases [29], and gases in low dimensions [30,31]. Other experiments strive for the realization of quantum information processors [32–34]. The high sensitivity and micron-scale position control have been used for probing static magnetic [35] and electric [36] fields as well as microwaves [37]. Creating atom interferometers [38] on atom chips is equally appealing. Here, an on-chip high stability atomic clock not only provides an excellent candidate for mobile timing applications, it also takes a pioneering role among this broad range of atom chip experiments, demonstrating that experimental parameters can be mastered to the fundamental physics limit.

This paper is organized as follows: We first describe the atomic levels and the experimental setup. Then we give the evaluation of the clock stability and an analysis of all major noise sources.

II. ATOMIC LEVELS

We interrogate the hyperfine transition of ^{87}Rb (Fig. 1). A two-photon drive couples the magnetically trappable states $|1\rangle \equiv |F=1,m_F=-1\rangle$ and $|2\rangle \equiv |F=2,m_F=1\rangle$, whose transition frequency exhibits a minimum at a magnetic field near $B_m \approx 3.229$ G [39,40]. This second-order dependence strongly reduces the clock frequency sensitivity to

*Peter.Rosenbusch@obspm.fr

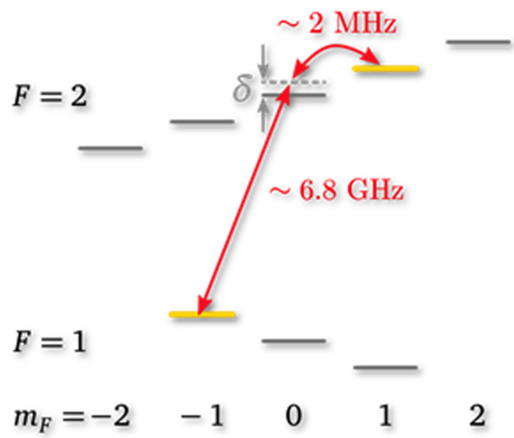

FIG. 1. (Color online) Level scheme of the ^{87}Rb ground state. The two magnetically trappable clock states $|F = 1, m_F = -1\rangle$ and $|F = 2, m_F = 1\rangle$ are coupled via a two-photon, microwave and radiofrequency transition, where the microwave is tuned 500 kHz above the $|1,-1\rangle \rightarrow |2,0\rangle$ transition.

magnetic field fluctuations. It assures that atoms with different trajectories within the trap still experience similar Zeeman shifts. Furthermore, by tuning the offset magnetic field, the inhomogeneity from the negative collisional shift [40] can be compensated to give a quasi-position-invariant overall shift [41]. Under these conditions of strongly reduced inhomogeneity we have shown that spin self-rephasing can overcome dephasing and that coherence times of 58 ± 12 s [11] can be reached. It confirms the possibility to create a high stability clock [42].

III. EXPERIMENTAL SETUP

The experimental setup, details of which are given in [43], is similar to compact atom chip experiments reported previously [44,45]. All experimental steps, laser cooling, evaporative cooling, interrogation, and detection take place in an $\sim$(5 cm)^3 glass cell where one cell wall is replaced by the atom chip (Fig. 2). In this first-generation setup, a 25-l/s

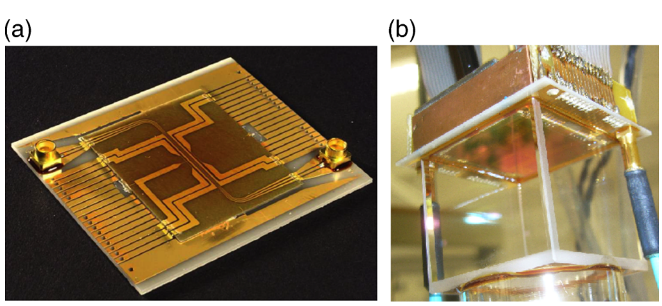

FIG. 2. (Color online) (a) The implemented atom chip. One identifies the Z-shaped coplanar waveguide which serves for atom trapping and transport of the microwave interrogation signal. The outer dimensions are 38×45.5 mm^2. (b) The chip constitutes one of the facets of the vacuum cell facilitating electrical contact. The cell is surrounded by a $10 \times 10 \times 15$ cm^3 cage of Helmholtz coils and a 30-cm diameter optical table holding all optical beam expanders. The cell is evacuated via standard UHV equipment.

TABLE I. Timing sequence of one experimental cycle. The total cycle time is 16 s.

Operation	Duration
MOT	6.85 s
Compressed MOT	20 ms
Optical molasses	5 ms
Optical pumping	1 ms
Magnetic trapping and compression	230 ms
RF evaporation	3 s
Magnetic decompression	700 ms
First Ramsey pulse	77.65 ms
Ramsey time	5 s
Second Ramsey pulse	77.65 ms
Time of flight ($|1\rangle$, $|2\rangle$)	(5.5, 8.5) ms
Detection	20 μs

ion pump is connected via standard vacuum components. It evacuates the cell to a pressure of $\sim 1 \times 10^{-9}$ mbar. The cell is surrounded by a $10 \times 10 \times 15$ cm^3 cage of Helmholtz coils. A 30-cm diameter optical table holds the coil cage as well as all beam expanders necessary for cooling and detection and is surrounded by two layers of magnetic shielding.

The timing sequence (Table I) starts with a mirror MOT [44] loading $\sim 3 \times 10^6$ atoms in $\sim$7 s from the background vapor. The MOT magnetic field is generated by one of the coils and a U-shaped copper structure placed behind the atom chip [46]. Compressing the MOT followed by 5 ms optical molasses cools the atoms to $\sim$20 μK. The cloud is then optically pumped to the $|1\rangle$ state and transferred to the magnetic trap. It is gradually compressed to perform RF evaporation, which takes $\sim$3 s. A 0.7-s decompression ramp transfers the atoms to the final interrogation trap with trap frequencies $(\omega_x, \omega_y, \omega_z) = 2\pi \times (2.7, 92, 74)$ Hz located 350 μm below the surface. It is formed by two currents on the chip and two currents in two pairs of Helmholtz coils. The currents are supplied by home-built current supplies with relative stability $< 10^{-5}$ at 3 A [47]. The final atom number is $N = 2 - 4 \times 10^4$ and their temperature $T \sim 80$ nK. The density is thus with $\bar{n} \approx 1.5 \times 10^{11}$ atoms/cm^3 so low that the onset of Bose-Einstein condensation would occur at 5 nK. With $k_B T/\hbar\omega_{x,y,z} > 20$ the ensemble can be treated by the Maxwell-Boltzmann distribution. The trap lifetime $\gamma^{-1} = 6.9$ s is limited by background gas collisions. The clock transition is interrogated via two-photon (microwave + radiofrequency) coupling, where the microwave is detuned 500 kHz above the $|1\rangle$ to $|F = 2, m_F = 0\rangle$ transition (Fig. 1). The microwave is coupled to a three-wire coplanar waveguide on the atom chip [43,45]. The interaction of the atoms with the waveguide evanescent field allows one to reach single-photon Rabi frequencies of a few kHz with moderate power $\sim$0 dBm. Since the microwave is not radiated, interference from reflections, that can lead to field zeros and time varying phase at the atom position, is avoided. Thereby, the waveguide avoids the use of a bulky microwave cavity. The microwave signal of fixed frequency $\nu_{\mathrm{MW}} \sim 6.8$ GHz is generated by a home-built synthesizer [48] which multiplies a 100-MHz reference signal derived from an active hydrogen maser [49] to the microwave frequency without degradation of the maser phase noise. The actual phase noise is detailed in Sec. V B. The RF signal of variable frequency $\nu_{\mathrm{RF}} \sim 2$ MHz comes from a commercial DDS which supplies a "standard" wire parallel to the waveguide. The two-photon Rabi frequency is about $\Omega = 3.2$ Hz making a $\pi/2$ pulse last $\tau_p = 77.65$ ms $\gg 2\pi/\omega_z$. The pulse duration is chosen so that any Rabi frequency inhomogeneity, which was characterized in [50], is averaged out and Rabi oscillations show 99.5% contrast. Two pulses enclose a Ramsey time of $T_R = 5$ s. Detection is performed via absorption imaging. A strongly saturating beam crosses the atom cloud and is imaged onto a back illuminated, high quantum efficiency CCD camera with frame transfer (Andor iKon M 934-BRDD). Illumination (20 μs) without and with repump light, 5.5 ms and 8.5 ms after trap release, probes the $F = 2$ and $F = 1$ atoms independently. Between these two, a transverse laser beam blows away the $F = 2$ atoms. Numerical frame re-composition generates the respective reference images and largely reduces the effect of optical fringes [51]. Calculation of the optical density and correction for the high saturation [52] give access to the atom column density. The so found two-dimensional (2D) atom distributions are fitted by Gaussians to extract the number of atoms in each state $N_{1,2}$. The transition probability is calculated as $P = N_2/(N_1 + N_2)$ accounting for total atom number fluctuations. The actual detection noise is discussed in Sec. V A. The total time of one experimental cycle is $T_c = 16$ s.

IV. STABILITY MEASUREMENT

Prior to any stability measurement we record the typical Ramsey fringes. We repeat the experimental cycle while scanning $\nu_{\mathrm{LO}} = \nu_{\mathrm{MW}} + \nu_{\mathrm{RF}}$ over $\sim$3 fringes. Doing so for various Ramsey times T_R allows one to identify the central fringe corresponding to the atomic frequency ν_{at}. Figure 3 shows typical fringes for $T_R = 5$ s, where each point is a single shot. One recognizes the Fourier limited linewidth of 100 mHz equivalent to $\sim 10^{11}$ quality factor. The 85% contrast is remarkable. A sinusoidal fit gives the slope at the fringe half-height $dP/d\nu = 13.4$/Hz, which is used in the

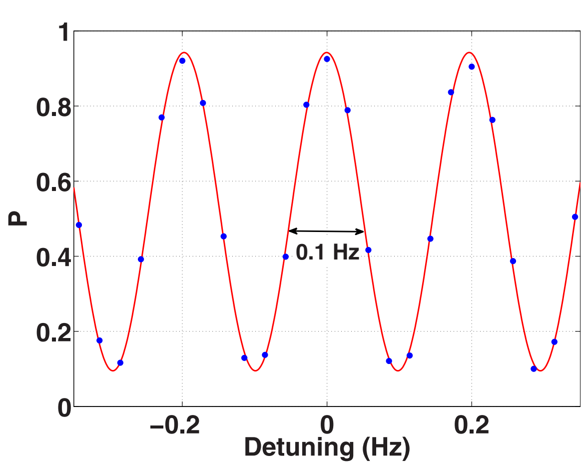

FIG. 3. (Color online) Typical Ramsey fringes recorded at $T_R = 5$ s while scanning the local oscillator detuning. Each point corresponds to a single experimental realization. One identifies the Fourier limited linewidth of 100 mHz and the very good contrast of 85%.

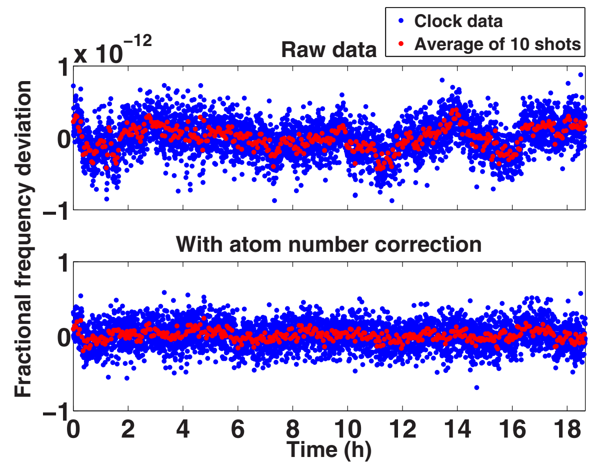

FIG. 4. (Color online) Relative frequency deviation when repeating the clock measurement over 18 h, (top) raw data, (bottom) after correction by the simultaneously detected total atom number. The blue dots represent single shots; red dots show an average of 10 shots.

following stability evaluation to convert the detected transition probability into frequency.

Evaluation of the clock stability implies repeating the experimental cycle several thousand times. The clock is free running, i.e., we measure the transition probability at each cycle, but we do not feedback to the interrogation frequency ν_{LO}. Only an alternation in successive shots from a small fixed negative to positive detuning, $\Delta_{\mathrm{mod}}/(2\pi) = \pm 50$ mHz, probes the left and right half-height of the central fringe. The difference in P between two shots gives the variation of the central frequency independent from long-term detection or microwave power drifts. In the longest run, we have repeated the frequency measurement over 18 h.

The measured frequency data is traced in Fig. 4 versus time. Besides shot-to-shot fluctuations one identifies significant long-term variations. Correction of the data with the atom number, by a procedure we will detail in Sec. V C 1, results in substantial improvement. We analyze the data by the Allan standard deviation which is defined as [53]

$$\sigma_y^2(\tau) \equiv \frac{1}{2} \sum_{k=1}^{\lfloor L/2^l \rfloor - 1} (\bar{y}_{k+1} - \bar{y}_k)^2. \qquad (1)$$

Here L is the total number of data points and the $\bar{y}_k$ are averages over packets of 2^l successive data points with $l \in \{0,1,\dots \lfloor \log_2 L \rfloor\}$ and $\tau = 2^l T_c$. Figure 5 shows the Allan standard deviation of the uncorrected and corrected data. For $0 \leqslant l \leqslant 9$ the points and their error bars are plotted as calculated with the software STABLE32 [54]. This software uses Eq. (1) to find the points. The error bars are calculated as the 5%–95% confidence interval based on the appropriate χ^2 distribution. The software stops output at $l = \lfloor \log_2 L \rfloor - 2$ since there are too few differences $\bar{y}_{k+1} - \bar{y}_k$ to give a statistical error bar. Instead we directly plot all differences for $l = 10$ and 11.

The Allan standard deviation shows the significant improvement brought by the atom number correction. The uncorrected data starts at $\tau = T_c = 16$ s with $\sigma_y = 1.9 \times 10^{-13}$

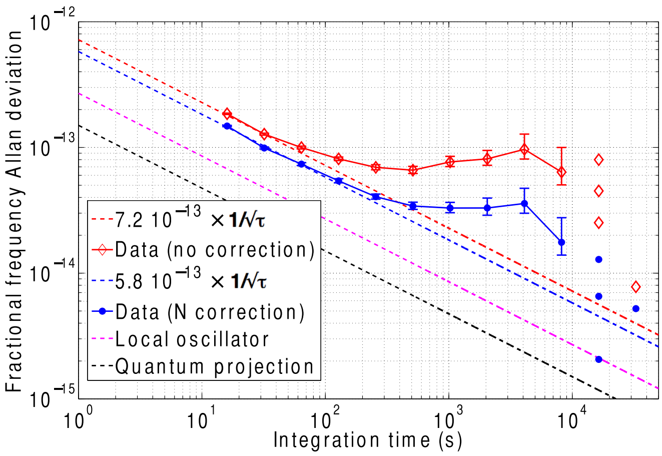

FIG. 5. (Color online) Allan standard deviation of the measured clock frequency with (blue circles) and without (red diamonds) atom number correction. For integration times smaller than 10^4 s, the points and error bars are calculated using the software STABLE32. Above 10^4 s, the individual differences between successive packets of 1024 and 2048 measurements are given. The N-corrected data follows initially $5.8 \times 10^{-13}\tau^{-1/2}$ (blue dashed line). The quantum projection noise and the local oscillator noise are given for reference.

shot-to-shot. For the N-corrected data, the shot-to-shot stability is $\sigma_y = 1.5 \times 10^{-13}$. Up to $\tau \approx 100$ s the corrected frequency fluctuations follow a white noise behavior of $\sigma_y(\tau) = 5.8 \times 10^{-13}\tau^{-1/2}$. At $\tau \approx 1000$ s, the fluctuations are above the $\tau^{-1/2}$ behavior but decrease again at $\tau > 5000$ s. For $\tau > 10^4$ s, three of the four individual differences are below 10^{-14}. This lets us expect that a longer stability evaluation would indeed confirm a stability in the 10^{-15} range with sufficient statistical significance. The "shoulder" above the white noise behavior is characteristic for an oscillation at a few 10^3-s half-periods. Indeed, this oscillation is visible in the raw data in Fig. 4. Its cause is yet to be identified through simultaneous tracking of many experimental parameters—a task which goes beyond the scope of this paper.

Table II gives a list of identified shot-to-shot fluctuations that contribute to the clock frequency noise. Treating them as statistically independent and summing their squares gives a fractional frequency fluctuation of 1.5×10^{-13} shot-to-shot or 6.0×10^{-13} at 1 s, corresponding to the measured stability. We have thus identified all major noise sources building a solid basis for future improvements. In the following we discuss each noise contribution in detail.

TABLE II. List of identified contributions to the clock (in)stability. Atom temperature fluctuations dominate followed by magnetic field fluctuations and local oscillator noise. The quadratic sum of all contributions explains the measured stability.

Relative frequency stability (10^{-13})	Shot-to-shot	At 1 s
Measured, without correction	2.0	7.2
Measured, after N correction	**1.5**	**5.8**
Atom temperature	1.0	3.9
Magnetic field	0.7	2.6
Local oscillator	0.7	2.7
Quantum projection	0.4	1.5
N correction	0.4	1.5
Atom loss	0.3	1.1
Detection	0.3	1.1
Total estimate	1.5	6.0

V. NOISE ANALYSIS

In a passive atomic clock, an electromagnetic signal generated by an external local oscillator (LO) interacts with an atomic transition. The atomic transition frequency ν_{at} is probed by means of spectroscopy. The detected atomic excitation probability P is either used to correct the LO online such that $\nu_{LO} = \nu_{at}$, or, as applied here, the LO is left free running and the measured differences $(\nu_{LO} - \nu_{at})(t)$ are recorded for post-treatment. The so calibrated LO signal is the useful clock output.

When concerned with the stability of the output frequency, we have to analyze the noise of each element within this feedback loop, i.e., as below.

(A.) Noise from imperfect detection.

(B.) Folded-in fluctuations of the LO frequency known as Dick effect.

(C.) Fluctuations of the atomic transition frequency induced by interactions with the environment or between the atoms.

We begin by describing the most intuitive contribution (A. detection noise) and finish by the most subtle (C. fluctuations of the atomic frequency).

A. Detection and quantum projection noise

The clock frequency is deduced from absorption imaging the atoms in each clock state as described in Sec. III. N_1 and N_2 are obtained by fitting Gaussians to the atom distribution, considering a square region of interest of $\sim 3 \times 3$ cloud widths.

Photon shot noise and optical fringes may lead to atom number fluctuations of standard deviation σ_{det}. These fluctuations add to the true atom number. Analyzing blank images, we confirm that σ_{det}^2 increases as the number of pixels in the region of interest and that optical fringes have been efficiently suppressed [51]. This scaling has led to the choice of short times of flight where the atoms occupy fewer pixels [55]. Supposing the same σ_{det} for both states, we find for the transition probability noise $\sigma_{P,det} = \sigma_{det}/(\sqrt{2}N)$ with $N = N_1 + N_2$.

Another P degradation may occur if the Rabi frequency of the first pulse fluctuates or if the detection efficiency varies between the $|1\rangle$ and $|2\rangle$ detection. The latter may arise from fluctuations of the detection laser frequency on the time scale of the 3-ms difference in time of flight. Both fluctuations induce a direct error $\sigma_{P,\mathrm{Rf+lf}}$ on P independent from the atom number.

Quantum projection noise is a third cause for fluctuations in P. This fundamental noise arises from the fact that the detection projects the atomic superposition state onto the base states. Before detection, the atom is in a near-equal superposition of $|1\rangle$ and $|2\rangle$. The projection then can result in either base state with equal probability giving $\sigma_{QPN} = 1/2$ for one atom. Running the clock with N (nonentangled) atoms is equivalent to N successive measurement resulting in $\sigma_{P,QPN} = 1/(2\sqrt{N})$ shot-to-shot.

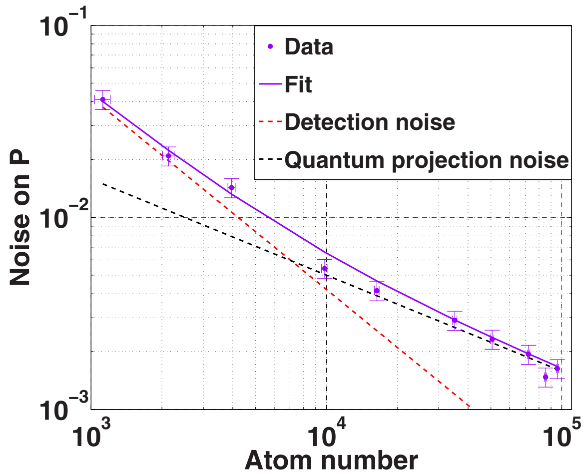

FIG. 6. (Color online) Characterization of the detection noise. Only a single $\pi/2$ pulse is applied and $P = N_2/N$ detected. The shot-to-shot Allan deviation is plotted as a function of the total atom number. We fit the data with the quadratic sum of the detection noise $\sigma_{\rm det}/(\sqrt{2}N)$, the quantum projection noise $1/(2\sqrt{N})$, and the Rabi frequency and laser frequency noise $\sigma_{P,\rm Rf+lf}$. The fit gives $\sigma_{\rm det} = 59$ atoms and $\sigma_{P,\rm Rf+lf} < 10^{-4}$.

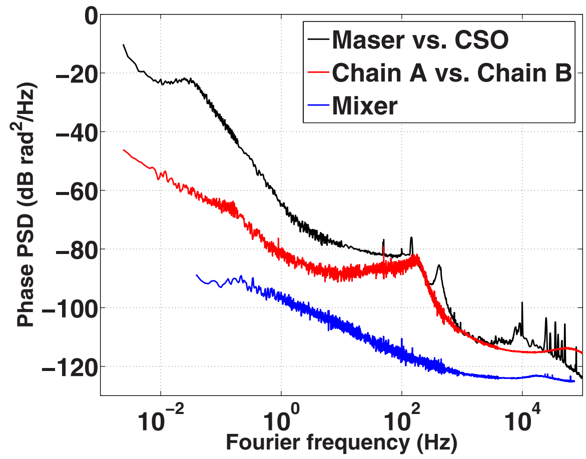

FIG. 7. (Color online) Phase noise power spectral density of the local oscillator. The frequency multiplication chain and the 100-MHz reference signal are characterized separately. The beat between two quasi-identical chains is performed at 6.8 GHz (red). The beat of the reference signal against a cryogenic sapphire oscillator is taken at 100 MHz and scaled to 6.8 GHz (black). The noise of the reference signal dominates in the low frequency part, where our clock is sensitive. Both results are above the intrinsic noise of the measurement system (blue).

We quantify the above three noise types from an independent measurement: Only the first $\pi/2$ pulse is applied and P is immediately detected. The measurement is repeated for various atom numbers and $\sigma_P(N)$ is extracted. Figure 6 shows the measured σ_P shot-to-shot versus N. Considering the noise sources as statistically independent, we fit the data by $\sigma_P^2 = \sigma_{\rm det}^2/(2N^2) + 1/(4N) + \sigma_{P,\rm RF+lf}^2$ and find $\sigma_{\rm det} = 59$ atoms and $\sigma_{P,\rm RF+lf} < 10^{-4}$. $\sigma_{\rm det}$ is equivalent to an average of 2.2 atoms/pixel for our very typical absorption imaging system. The low $\sigma_{\rm RF+lf}$ proves an excellent passive microwave power stability $< 2.5 \times 10^{-4}$, which may be of use in other experiments, in particular microwave dressing [56,57].

During the stability measurement of Fig. 4 about 20 000 atoms are detected, which is equivalent to $\sigma_{y,\rm QPN} = 0.4 \times 10^{-13}$ shot-to-shot. The detection region of interest is slightly bigger than for the above characterization, so that $\sigma_{\rm det} = 69$ atoms, corresponding to $\sigma_{y,\rm det} = \sigma_{\rm det}(\nu_{\rm at}N)^{-1}|dP/d\nu|^{-1} = \frac{\sigma_{\rm det}}{\sqrt{2}N}\frac{1}{\nu_{\rm at}13.4} = 0.3 \times 10^{-13}$ shot-to-shot. In both we have used $dP/d\nu$ as measured in Fig. 3.

B. Local oscillator noise

The experimental cycle probes $\nu_{\rm at} - \nu_{\rm LO}$ only during the Ramsey time. Atom preparation and detection cause dead time. Repeating the experimental cycle then constitutes periodic sampling of the LO frequency and its fluctuations. This, as is well known from numerical data acquisition, leads to aliasing. It folds high Fourier frequency LO noise close to multiples of the sampling frequency $1/T_c$ back to low frequency variations, which degrade the clock stability. Thus even high Fourier frequency noise can degrade the clock signal. The degradation is all the more important as the dead time is long and the duty cycle $d = T_R/T_c$ is low. This stability degradation $\sigma_{y,\rm Dick}$ is known as the Dick effect [58]. It is best calculated using the sensitivity function $g(t)$ [59]: During dead time, $g = 0$ whereas during T_R, when the atomic coherence $|\psi\rangle = (|1\rangle + e^{i\phi}|2\rangle)/\sqrt{2}$ is fully established $g = 1$. During the first Ramsey pulse, when the coherence builds up, g increases as $\sin\Omega t$ for a square pulse and decreases symmetrically for the second pulse [60]. Then the interrogation outcome is

$$\delta\nu = \frac{\int_{-T_c/2}^{T_c/2}(\nu_{\rm at}(t) - \nu_{\rm LO}(t))g(t)\,dt}{\int_{-T_c/2}^{T_c/2}g(t)\,dt}, \quad (2)$$

with

$$g(t) = \begin{cases} a\sin\Omega(T_R/2 + \tau_p + t) & -\tau_p - \frac{T_R}{2} \leqslant t \leqslant -\frac{T_R}{2} \\ a\sin\Omega\tau_p & -\frac{T_R}{2} \leqslant t < \frac{T_R}{2} \\ a\sin\Omega(\frac{T_R}{2} + \tau_p - t) & \frac{T_R}{2} \leqslant t \leqslant \frac{T_R}{2} + \tau_p \\ 0 & \text{otherwise.} \end{cases} \quad (3)$$

Typically $\Omega\tau_p = \pi/2$ and, for operation at the fringe half-height, $a = \sin\Delta_{\rm mod}T_R = 1$. Because of the periodicity of repeated clock measurements, it is convenient to work in Fourier space with

$$g_l = \frac{1}{T_c}\int_{-T_c/2}^{T_c/2} g(t)\cos(2\pi l\, t/T_c)dt. \quad (4)$$

Using the power spectral density of the LO frequency noise $S_y^f(f)$ (see Fig. 7), the contribution to the clock stability becomes the quadratic sum over all harmonics [59],

$$\sigma_{y,\rm Dick}^2(\tau) = \frac{1}{\tau}\sum_{l=1}^{\infty}\left(\frac{g_l}{g_0}\right)^2 S_y^f(l/T_C). \quad (5)$$

Here we have assumed $\nu_{\rm at}$ constant in time; its fluctuations are treated in the next section. The coefficients $(g_l/g_0)^2$ are shown as points in Fig. 8 for our conditions. The weight of the first few harmonics is clearly the strongest, rapidly decaying

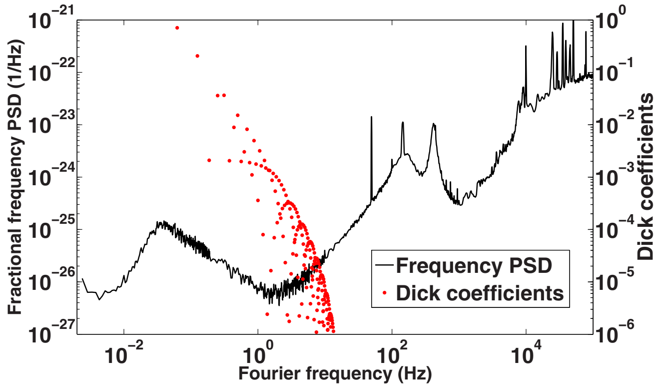

FIG. 8. (Color online) (black) Same data as Fig. 7 now expressed as fractional frequency fluctuations $S_y = f^2 S_\phi/\nu_{\rm MW}^2$. (Red) Fourier coefficients of the sensitivity function $(g_l/g_0)^2$ for our conditions ($T_c = 16$ s, $T_R = 5$ s and $\tau_p = 77.65$ ms). Multiplication of the two gives the stability degradation known as Dick effect.

over six decades in the range $1/T_c \approx 0.1$ Hz to $1/\tau_p \approx 10$ Hz. Above ~10 Hz the g_l are negligible.

To measure $S_y^f(f)$ we divide our LO into two principal components: the 100-MHz reference signal derived from the hydrogen maser and the frequency multiplication chain generating the 6.8-GHz interrogation signal. We characterize each independently by measuring the phase noise spectrum $S_\phi(f)$. The fractional frequency noise $S_y^f(f)$ is obtained from simple differentiation as $S_y^f(f) = f^2 S_\phi(f)/\nu_{\rm MW}^2$ [59]. The frequency noise of the RF signal can be neglected as its relative contribution is 3 orders of magnitude smaller.

We characterize the frequency multiplication chain by comparing it to a second similar model also constructed in-house. The two chains are locked to a common 100-MHz reference and their phase difference at 6.834 GHz is measured as a dc signal using a phase detector (Miteq DB0218LW2) and a FFT spectrum analyzer (SRS760). The measured $S_\phi(f)$ is divided by 2 assuming equal noise contributions from the two chains. It is shown in Fig. 7. It features a $1/f$ behavior up to $f = 10$ Hz and reaches a phase flicker floor of -115 dB rad^2/Hz at 1 kHz. The peak at $f = 200$ Hz is due to the phase lock of a 100-MHz quartz inside the chain to the reference signal. As we will see in the following, its contribution to the Dick effect is negligible.

The 100-MHz reference signal is generated by a 100-MHz quartz locked to a 5-MHz quartz locked with 40 mHz bandwidth to an active hydrogen maser (VCH-1003M). We measure this reference signal against a 100-MHz signal derived from a cryogenic sapphire oscillator (CSO) [61,62]. Now the mixer is M/A-COM PD-121. The CSO is itself locked to the reference signal but with a time constant of ~1000 s [63]. This being much longer than our cycle time, we can, for our purposes, consider the two as free running. The CSO is known from prior analysis [64] to be at least 10 dB lower in phase noise than the reference signal for Fourier frequencies higher than 0.1 Hz. Thus the measured noise can be attributed to the reference signal for the region of the spectrum $f > 1/T_c$ where our clock is sensitive. The phase noise spectrum is shown in Fig. 7. For comparison it was scaled to 6.8 GHz by adding 37 dB. Several maxima characteristic of the several phase locks in the systems can be identified. At low Fourier frequencies, the reference signal noise is clearly above the chain noise. For all frequencies, both are well above the noise floor of our measurement system. The noise of the reference signal being dominant in the range $1/T_c$ to $1/\tau_p$, where our clock is sensitive, we neglect the chain noise in the following.

Using Eq. (5), we estimate the Dick effect contribution as $\sigma_{y,\rm Dick} = 2.7 \times 10^{-13}\tau^{-1/2}$. This represents the second biggest contribution to the noise budget (Table II). It is due to the important dead time and the long cycle time which folds in the LO noise spectrum where it is strongest. Improvement is possible, first of all, through reduction of the dead time which is currently dominated by the ~7-s MOT loading phase and the 3-s evaporative cooling. Options for faster loading include pre-cooling in a 2D MOT [65] or a single-cell fast pressure modulation [66]. Utilization of a better local oscillator like the cryogenic sapphire oscillator seems obvious but defies the compact design. Alternatively, generation of low phase noise microwaves from an ultrastable laser and femtosecond comb has been demonstrated by several groups [67–69] and ongoing projects aim at miniaturization of such systems [70]. If a quartz local oscillator remains the preferred choice, possibly motivated by cost, one long Ramsey time must be divided into several short interrogation intervals interlaced by nondestructive detection [71–73].

C. Fluctuations of the atomic frequency

1. Atom number fluctuation

Having characterized the fluctuations of the LO frequency, we now turn to fluctuations of the atomic frequency. We begin by atom number fluctuations. Due to the trap confinement and the ultracold temperature, the atom density is 4 orders of magnitude higher than what is typically found in a fountain clock. Thus the effect of atom-atom interactions on the atomic frequency must be taken into account even though ^{87}Rb presents a substantially lower collisional shift than the standard ^{133}Cs. Indeed, when plotting the measured clock frequency against the detected atom number $N = N_1 + N_2$, which fluctuates by 2%–3% shot-to-shot, we find a strong correlation (Fig. 9). The distribution is compatible with a linear fit with slope $k = -2.70(7)$ μHz/atom. In order to confirm this value with a theoretical estimate we use the mean-field approach and the s-wave scattering lengths a_{ij} which depend on the atomic states only [40]:

$$\Delta\nu_C(\vec{r}) = \frac{2\hbar}{m} n(\vec{r})[(a_{22} - a_{11}) + (2a_{12} - a_{11} - a_{22})\theta], \tag{6}$$

where $n(\vec{r})$ is the position-dependent density and $a_{11} = 100.44a_0$, $a_{22} = 95.47a_0$, and $a_{12} = 98.09a_0$ are the scattering lengths with $a_0 = 0.529 \times 10^{-10}$ m [40]. We assume perfect $\pi/2$ pulses and so $\theta \equiv (N_1 - N_2)/N = 0$. Integrating over the Maxwell-Boltzmann density distribution we get

$$\overline{\Delta\nu_C} = N\frac{-\hbar(a_{11} - a_{22})\sqrt{m}\omega_x\omega_y\omega_z}{4(\pi k_B T)^{3/2}}. \tag{7}$$

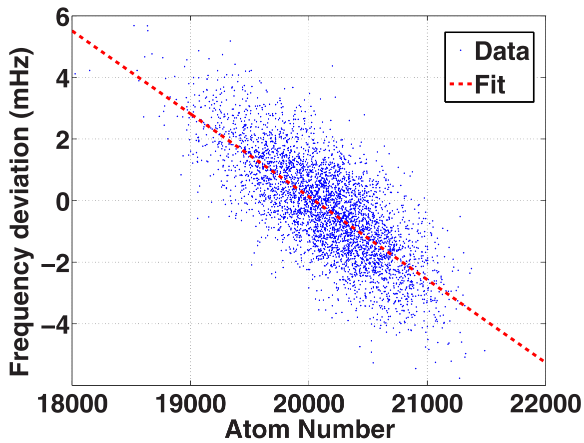

FIG. 9. (Color online) Correlation between the detected atom number and the clock frequency for the data of Fig. 4. Fitting with a linear regression gives $k = -2.70(7)$ μHz/atom, which allows one to correct the clock frequency at each shot and yields substantial stability improvement.

We must consider that the atom number decays during the $T_R = 5$ s since the trap lifetime is $\gamma^{-1} = 6.9$ s. We replace N by its temporal average,

$$\overline{N} = \frac{1}{T_R}\int_0^{T_R} N_i e^{-\gamma t} dt = N_i \frac{1 - e^{-\gamma T_R}}{\gamma T_R}$$
$$= N_f \frac{e^{\gamma T_R} - 1}{\gamma T_R} \approx 1.47\, N_f, \tag{8}$$

where N_i and N_f are the initial and final atom numbers, respectively. Note that N_f is the detected atom number. Using $T = 80$ nK, which is compatible with an independent measurement, we recover the experimental collisional shift of $k = -2.7$ μHz/(detected atom). It is equivalent to an overall collisional shift of $\overline{\Delta\nu_C} = -54$ mHz for $N_f = 20\,000$.

Using k and the number of atoms detected at each shot we can correct the clock frequency for fluctuations. The corrected frequency is given in Fig. 4 showing a noticeable improvement in the short-term and long-term stability. The Allan deviation indicates a clock stability of $5.8 \times 10^{-13}\tau^{-1/2}$ at short term as compared to $7.2 \times 10^{-13}\tau^{-1/2}$ for the uncorrected data. At long term the improvement is even more pronounced. This demonstrates the efficiency of the N correction. Furthermore, the experimentally found k shows perfect agreement with our theoretical prediction so that the theoretical coefficient can in the future be used from the first shot on without the need for post-treatment.

While we have demonstrated the efficiency of the atom number correction, the procedure has imperfections for two reasons: The first, of technical origin, are fluctuations in the atom number detectivity as evaluated in Sec. V A. The second arises from the fact that atom loss from the trap is a statistical process. For the first, we get $\sigma_{y,\text{correction}} = \sqrt{2}|k|\sigma_{\text{det}}/\nu_{\text{at}} = 0.4 \times 10^{-13}$ shot-to-shot. This value is well below the measured clock stability, but may become important when other noise sources are eliminated. It can be improved by reducing the atom density and thus k or by better detection, in particular at shorter time of flight where the camera region of interest can be smaller. The second cause, the statistical nature of atom loss, translates into fluctuations that in principle cannot be corrected. The final atom number N_f at the end of the Ramsey time is known from the detection, but the initial atom number N_i can only be retraced with a statistical error. To estimate this contribution we first consider the decay from the initial atom number N_i. At time t, the probability for a given atom to still be trapped is $e^{-\gamma t}$ and the probability to have left the trap is $1 - e^{-\gamma t}$. Given N_i, the probability p to have N_t atoms at t is proportional to $e^{-N_t\gamma t}(1 - e^{-\gamma t})^{N_i - N_t}$ and to the number of possible combinations:

$$p(N_t \text{ given } N_i) = \frac{N_i!}{N_t!(N_i - N_t)!} e^{-N_t\gamma t}(1 - e^{-\gamma t})^{N_i - N_t}. \tag{9}$$

The sum of this binomial distribution over all $0 \leqslant N_t \leqslant N_i$ is by definition normalized. We are interested in the opposite case: Since we detect N_f at $t = T_R$, we search the probability of N_t given N_f.

$$p(N_t \text{ given } N_f) = \frac{A N_t!}{N_f!(N_t - N_f)!} \times e^{-N_f\gamma(T_R - t)}(1 - e^{-\gamma(T_R - t)})^{N_t - N_f}. \tag{10}$$

The combinatorics are as in Eq. (9) when replacing $N_t \to N_f$ and $N_i \to N_t$, but now normalization sums over $0 \leqslant N_t < \infty$. Here it is convenient to approximate the binomial distribution by the normal distribution,

$$p(N_t \text{ given } N_f) \approx \frac{A}{\sqrt{2\pi\eta}} e^{-(N_f - N_t e^{-\gamma(T_R - t)})^2/(2\eta)}, \tag{11}$$

with $\eta = N_t e^{-\gamma(T_R - t)}(1 - e^{-\gamma(T_R - t)})$ and hence $A = e^{-\gamma(T_R - t)}$. Then, the mean of N_t is

$$\langle N_t \rangle = (N_f + 1)e^{\gamma(T_R - t)} - 1 \approx N_f e^{\gamma(T_R - t)}, \tag{12}$$

and its statistical error,

$$\sigma_{N_t} = \sqrt{(1 - e^{\gamma(T_R - t)})(2 - (N_f + 2)e^{\gamma(T_R - t)})}$$
$$\approx \sqrt{N_f(e^{\gamma(T_R - t)} - 1)e^{\gamma(T_R - t)}}. \tag{13}$$

Setting $t = 0$, we get $\sigma_{N_i} = 210$. Integrating σ_{N_t} over T_R gives $\overline{\sigma_N} = 113 \approx \sigma_{N_i}/2$ and a frequency fluctuation of $\sigma_{y,\text{losses}} = 0.3 \times 10^{-13}$ shot-to-shot. This can be improved by increasing the trap lifetime well beyond the Ramsey time, which for our setup implies better vacuum with lower background pressure. Alternatively one can perform a nondestructive measurement of the initial atom number [74]. Assuming an error of 80 atoms on such a detection would decrease the frequency noise to $\sigma_{y,\text{losses}} = 0.1 \times 10^{-13}$ shot-to-shot.

2. *Magnetic field and atom temperature fluctuations*

We have analyzed the effect of atom number fluctuations. Two other parameters strongly affect the atomic frequency: the atom temperature and the magnetic field. We show that their influence can be evaluated by measuring the clock stability for different magnetic fields at the trap center. We begin by modeling the dependence of the clock frequency.

Our clock operates near the magic field $B_m \approx 3.229$ G for which the transition frequency has a minimum of -4497.31 Hz with respect to the field free transition,

$$\Delta\nu_B(\vec{r}) = b(B(\vec{r}) - B_m)^2, \quad (14)$$

with $b \approx 431$ Hz/G^2. For atoms trapped in a harmonic potential in the presence of gravity, the Zeeman shift becomes position dependent,

$$\Delta\nu_B(\vec{r}) = \frac{bm^2}{\mu_B^2}\left(\omega_x^2x^2 + \omega_y^2y^2 + \omega_z^2z^2 - 2gz + \delta B\frac{\mu_B}{m}\right)^2, \quad (15)$$

with $\delta B \equiv B(\vec{r}=0) - B_m$ and g the gravitational acceleration [41]. Using the Maxwell-Boltzmann distribution the ensemble averaged Zeeman shift is

$$\overline{\Delta\nu_B} = \frac{b}{\mu_B^2}\left(\frac{4g^2mk_BT}{\omega_z^2} + 15k_B^2T^2 + 6\mu_B\delta Bk_BT + \delta B^2\mu_B^2\right). \quad (16)$$

Differentiation with respect to δB leads to the effective magic field,

$$\delta B_0^B = \frac{-3k_BT}{\mu_B}, \quad (17)$$

where the ensemble averaged frequency is independent from magnetic field fluctuations. For $T = 80$ nK, $\delta B_0^B = -3.6$ mG whose absolute value almost coincides with the magnetic field inhomogeneity across the cloud, $(\overline{B(\vec{r})^2 - \overline{B}^2})^{1/2} = \sqrt{6}k_BT/\mu_B = 2.92$ mG. δB_0^B is close to the field of maximum contrast $\delta B_0^C \approx -40$ mG such that the fringe contrast is still 85% (Fig. 10).

If $\delta B \neq \delta B_0^B$ is chosen the clock frequency fluctuations due to magnetic field fluctuations are

$$\sigma_{y,B} = \frac{2b}{\nu_{at}}\left|\delta B_0^B - \delta B\right|\sigma_B. \quad (18)$$

We will use this dependence to measure σ_B.

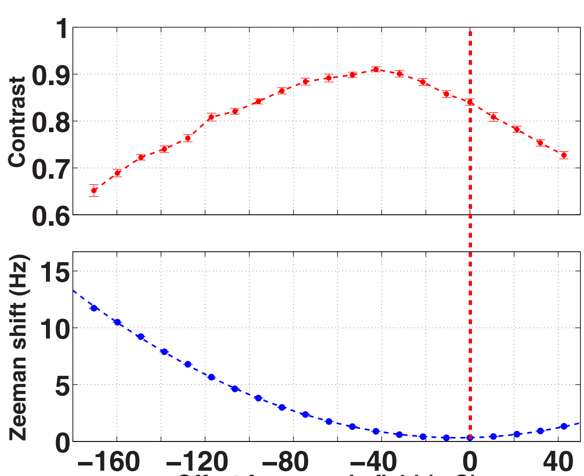

FIG. 10. (Color online) Fringe contrast (top) and differential Zeeman shift (bottom) of the clock frequency with respect to the frequency minimum for various magnetic fields. $\delta B = 0$ indicates the magic field of 3.229 G. The contrast maximum is offset by −40 mG.

Temperature fluctuations affect the range of magnetic fields probed by the atoms and the atom density, i.e., the collisional shift. Differentiation of both with respect to temperature also leads to an extremum, where the clock frequency is insensitive to temperature fluctuations. The extremum puts a concurrent condition on the magnetic field with

$$\delta B_0^T = -\frac{15k_BT + \frac{2g^2m}{\omega_z^2}}{3\mu_B} - \frac{\hbar(a_{11} - a_{22})(e^{\gamma T_R} - 1)\sqrt{m}N_f\mu_B\omega_x\omega_y\omega_z}{16\pi^{3/2}b(k_BT)^{5/2}\gamma T_R}. \quad (19)$$

For our conditions, $\delta B_0^B = -3.6$ mG and $\delta B_0^T = -79$ mG are not identical but close and centered around δB_0^C. We will see in the following that a compromise can be found where the combined effect of magnetic field and temperature fluctuations is minimized. A "doubly magic" field cannot be found as always $\delta B_0^T < \delta B_0^B$, but lower T reduces their difference. If $\delta B \neq \delta B_0^T$ is chosen, the clock frequency fluctuations due to temperature fluctuations are

$$\sigma_{y,T} = \frac{6bk_B}{\mu_B\nu_{at}}\left|\delta B_0^T - \delta B\right|\sigma_T, \quad (20)$$

thus varying δB allows to measure σ_T, too.

We determine σ_B and σ_T experimentally by repeating several stability measurements for different δB over a range of 200 mG where the contrast is above 70%. The shot-to-shot stability is shown in Fig. 11. One identifies a clear minimum of the instability at $\delta B \approx -35$ mG, which coincides with δB_0^C and is a compromise between the two optimal points δB_0^T and δB_0^B. This means that both magnetic field and temperature fluctuations are present with roughly equal weight. We model

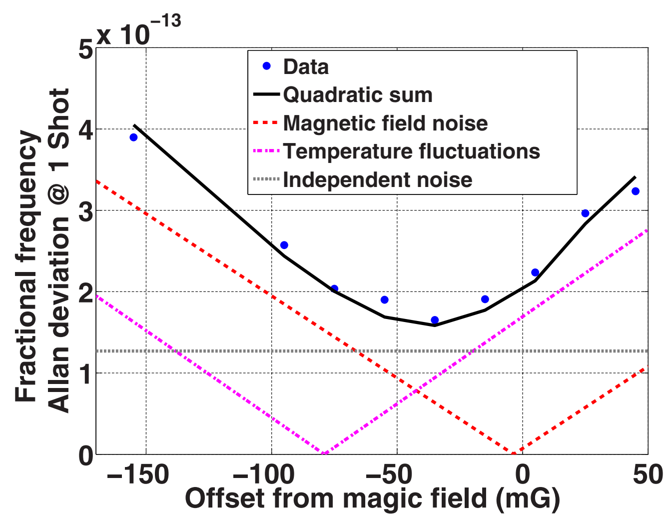

FIG. 11. (Color online) Shot-to-shot clock stability for various magnetic fields. Error bars are smaller than the point size. One observes a clear optimum at $\delta B = -35$ mG. Fitting with the quadratic sum of all identified noise contributions allows one to quantify the atom temperature fluctuations (0.4 nK shot-to-shot) and magnetic field fluctuations (16 μG shot-to-shot). The individual contributions are shown as dashed lines. Two sweet spots exist where the temperature dependence and the magnetic field dependence vanish.

the data with a quadratic sum of all so far discussed noise sources. Most of them give a constant offset; the slight variation due to the contrast variation shown in Fig. 10 is negligible. $\sigma_{y,B}$ and $\sigma_{y,T}$ are fitted by adjusting σ_B and σ_T. We find shot-to-shot temperature fluctuations of $\sigma_T = 0.44$ nK or 0.55% relative to 80 nK. The shot-to-shot magnetic field fluctuations are $\sigma_B = 16\ \mu$G or 5×10^{-6} in relative units. The values demonstrate our exceptional control of the experimental apparatus. Because the ambient magnetic field varies by <10 mG and the lowest magnetic shielding factor is 3950, we attribute σ_B to the instability of our current supplies. Indeed, it is compatible with the measured relative current stability [47]. The atom temperature fluctuations are small compared to a typical experiment using evaporative cooling. This may again be due to the exceptional magnetic field stability, since the atom temperature is determined by the magnetic field at the trap bottom during evaporation and the subsequent opening of the magnetic trap. At all stages, the current control is the most crucial. Using Eqs. (18) and (20), the temperature and magnetic field fluctuations translate into a frequency noise of $\sigma_{y,T} = 1.0 \times 10^{-13}$ and $\sigma_{y,B} = 0.7 \times 10^{-13}$ shot-to-shot, respectively. The comparison in Table II shows that these are the main sources of frequency instability together with the Dick effect. Therefore, improving the magnetic field and temperature noise is of paramount importance. The atom temperature can in principle be extracted from the absorption images, which we take at each shot. Analysis of the data set of Fig. 4 gives shot-to-shot fluctuations of $\sigma_T/T = 2 - 4\%$, which is much bigger than the 0.55% deduced above. We therefore conclude that the determination of the cloud width is overshadowed by a significant statistical error. Nevertheless, it needs to be investigated, whether better detection and/or imaging at long time of flight, may reduce this error. The magnetic field stability may be improved by refined power supplies, the use of multiwire traps [75], microwave dressing [57] or ultimately the use of atom chips with permanent magnetic material [76–78]. If the magnetic field fluctuations can be reduced, the temperature fluctuations may also reduce. Small σ_B would also allow one to operate nearer δB_0^T.

VI. CONCLUSION

We have built and characterized a compact atomic clock using magnetically trapped atoms on an atom chip. The clock stability reaches 5.8×10^{-13} at 1 s and is likely to integrate into the 10^{-15} range in less than a day. This is similar to the performance of the best compact atomic microwave clocks under development. It furthermore demonstrates the high degree of technical control that can be reached with atom chip experiments. After correction for atom number fluctuations, variations of the atom temperature and magnetic field are the dominant causes of the clock instability together with the local oscillator noise. The magnetic field stability may be improved by additional current sensing and feedback and ultimately by the use of permanent magnetic materials. This would allow one to operate nearer the second sweet spot where the clock frequency is independent from temperature fluctuations. The local oscillator noise takes an important role, because the clock duty cycle is <30%. We are now in the process of designing a second version of this clock, incorporating fast atom loading and nondestructive atom detection. We thereby expect to reduce several noise contributions to below $1 \times 10^{-13}\tau^{-1/2}$.

ACKNOWLEDGMENTS

We acknowledge fruitful discussion with P. Wolf, C. Texier, and P. Uhrich. We thank M. Abgrall and J. Guéna for the operation of the maser and the CSO. This work was supported within the European Metrology Research Programme (EMRP) under the project IND14. The EMRP is jointly funded by the EMRP participating countries within EURAMET and the European Union.

[1] C. N. Cohen-Tannoudji, Rev. Mod. Phys. **70**, 707 (1998).
[2] S. Chu, Rev. Mod. Phys. **70**, 685 (1998).
[3] W. D. Phillips, Rev. Mod. Phys. **70**, 721 (1998).
[4] M. A. Kasevich, E. Riis, S. Chu, and R. G. DeVoe, Phys. Rev. Lett. **63**, 612 (1989).
[5] A. Clairon, C. Salomon, S. Guellati, and W. Phillips, Europhys. Lett. **16**, 165 (1991).
[6] G. Santarelli, P. Laurent, P. Lemonde, A. Clairon, A. G. Mann, S. Chang, A. N. Luiten, and C. Salomon, Phys. Rev. Lett. **82**, 4619 (1999).
[7] J. M. Dow, R. Neilan, and C. Rizos, Geodes. **83**, 191 (2009).
[8] T. Ely, J. Seubert, J. Prestage, and R. Tjoelker, in *23rd Meeting on AAS/AIAA Spaceflight Mechanics 2013, Kauai, HI, United States* (AIAA, Reston, VA, 2013).
[9] H. Ott, J. Fortagh, G. Schlotterbeck, A. Grossmann, and C. Zimmermann, Phys. Rev. Lett. **87**, 230401 (2001).
[10] D. Harber, J. McGuirk, J. Obrecht, and E. Cornell, J. Low Temp. Phys. **133**, 229 (2003).
[11] C. Deutsch, F. Ramirez-Martinez, C. Lacroûte, F. Reinhard, T. Schneider, J.-N. Fuchs, F. Piéchon, F. Laloë, J. Reichel, and P. Rosenbusch, Phys. Rev. Lett. **105**, 020401 (2010).
[12] G. Kleine Büning, J. Will, W. Ertmer, E. Rasel, J. Arlt, C. Klempt, F. Ramirez-Martinez, F. Piéchon, and P. Rosenbusch, Phys. Rev. Lett. **106**, 240801 (2011).
[13] S. Bernon, H. Hattermann, D. Bothner, M. Knufinke, P. Weiss, F. Jessen, D. Cano, M. Kemmler, R. Kleiner, D. Koelle *et al.*, Nature Communications **4**, 2380 (2013).
[14] E. Burt, W. Diener, R. L. Tjoelker *et al.*, IEEE Transactions on Ultrasonics, Ferroelectrics, and Frequency Control **55**, 2586 (2008).
[15] R. Tjoelker, C. Bricker, W. Diener, R. Hamell, A. Kirk, P. Kuhnle, L. Maleki, J. Prestage, D. Santiago, D. Seidel *et al.*, in *Proceedings of the 1996 IEEE International Frequency Control Symposium (50th anniversary)* (IEEE, Piscataway, 1996), pp. 1073–1081.
[16] S. Kang, M. Gharavipour, C. Affolderbach, F. Gruet, and G. Mileti, J. Appl. Phys. **117**, 104510 (2015).
[17] S. Micalizio, C. Calosso, A. Godone, and F. Levi, Metrologia **49**, 425 (2012).
[18] J.-M. Danet, M. Lours, S. Guérandel, and E. de Clercq, IEEE Transactions on Ultrasonics, Ferroelectrics, and Frequency Control **61**, 567 (2014).

[19] F. Esnault, N. Rossetto, D. Holleville, J. Delporte, and N. Dimarcq, Adv. Space Res. **47**, 854 (2011).
[20] S. T. Müller, D. V. Magalhaes, R. F. Alves, and V. S. Bagnato, J. Opt. Soc. Am. B **28**, 2592 (2011).
[21] V. Shah, R. Lutwak, R. Stoner, and M. Mescher, in *Proceedings of IEEE International Frequency Control Symposium* (IEEE, Piscataway, 2012).
[22] E. Donley, E. Blanshan, F.-X. Esnault, and J. Kitching, in *2014 IEEE International Frequency Control Symposium* (IEEE, Piscataway, 2014), pp. 1–1.
[23] B. J. Bloom, T. L. Nicholson, J. R. Williams, S. L. Campbell, M. Bishof, X. Zhang, W. Zhang, S. L. Bromley, and J. Ye, Nature **506**, 71 (2014).
[24] N. Hinkley, J. Sherman, N. Phillips, M. Schioppo, N. Lemke, K. Beloy, M. Pizzocaro, C. Oates, and A. Ludlow, Science **341**, 1215 (2013).
[25] N. Poli, M. Schioppo, S. Vogt, U. Sterr, C. Lisdat, G. Tino *et al.*, Appl. Phys. B **117**, 1107 (2014).
[26] K. Bongs, Y. Singh, L. Smith, W. He, O. Kock, D. Świerad, J. Hughes, S. Schiller, S. Alighanbari, S. Origlia *et al.*, Comptes Rendus Physique **16**, 553 (2015).
[27] J. Reichel and V. Vuletic, *Atom Chips* (John Wiley & Sons, New York, 2011).
[28] W. Hänsel, P. Hommelhoff, T. Hänsch, and J. Reichel, Nature (London) **413**, 498 (2001).
[29] S. Aubin, S. Myrskog, M. Extavour, L. LeBlanc, D. McKay, A. Stummer, and J. Thywissen, Nature Physics **2**, 384 (2006).
[30] J. Estève, J.-B. Trebbia, T. Schumm, A. Aspect, C. I. Westbrook, and I. Bouchoule, Phys. Rev. Lett. **96**, 130403 (2006).
[31] S. Hofferberth, I. Lesanovsky, B. Fischer, T. Schumm, and J. Schmiedmayer, Nature (London) **449**, 324 (2007).
[32] J. Schmiedmayer, R. Folman, and T. Calarco, J. Mod. Opt. **49**, 1375 (2002).
[33] P. Treutlein, T. W. Hänsch, J. Reichel, A. Negretti, M. A. Cirone, and T. Calarco, Phys. Rev. A **74**, 022312 (2006).
[34] V. Leung, A. Tauschinsky, N. van Druten, and R. Spreeuw, Quant. Info. Proc. **10**, 955 (2011).
[35] S. Wildermuth, S. Hofferberth, I. Lesanovsky, E. Haller, L. M. Andersson, S. Groth, I. Bar-Joseph, P. Krüger, and J. Schmiedmayer, Nature (London) **435**, 440 (2005).
[36] A. Tauschinsky, R. M. T. Thijssen, S. Whitlock, H. B. van Linden van den Heuvell, and R. J. C. Spreeuw, Phys. Rev. A **81**, 063411 (2010).
[37] C. F. Ockeloen, R. Schmied, M. F. Riedel, and P. Treutlein, Phys. Rev. Lett. **111**, 143001 (2013).
[38] A. D. Cronin, J. Schmiedmayer, and D. E. Pritchard, Rev. Mod. Phys. **81**, 1051 (2009).
[39] M. R. Matthews, B. P. Anderson, P. C. Haljan, D. S. Hall, M. J. Holland, J. E. Williams, C. E. Wieman, and E. A. Cornell, Phys. Rev. Lett. **83**, 3358 (1999).
[40] D. M. Harber, H. J. Lewandowski, J. M. McGuirk, and E. A. Cornell, Phys. Rev. A **66**, 053616 (2002).
[41] P. Rosenbusch, Appl. Phys. B **95**, 227 (2009).
[42] P. Treutlein, P. Hommelhoff, T. Steinmetz, T. W. Hänsch, and J. Reichel, Phys. Rev. Lett. **92**, 203005 (2004).
[43] C. Lacroute, F. Reinhard, F. Ramirez-Martinez, C. Deutsch, T. Schneider, J. Reichel, and P. Rosenbusch, IEEE Trans. Ultrason. Ferroelectr. Freq. Control **57**, 106 (2010).
[44] J. Reichel, W. Hänsel, and T. W. Hänsch, Phys. Rev. Lett. **83**, 3398 (1999).
[45] P. Böhi, M. F. Riedel, T. W. Hänsch, and P. Treutlein, Appl. Phys. Lett. **97**, 051101 (2010).
[46] S. Wildermuth, P. Krüger, C. Becker, M. Brajdic, S. Haupt, A. Kasper, R. Folman, and J. Schmiedmayer, Phys. Rev. A **69**, 030901 (2004).
[47] F. Reinhard, Ph.D thesis, Design and construction of an atomic clock on an atom chip, Université Pierre et Marie Curie-Paris VI, 2009.
[48] F. Ramirez-Martinez, M. Lours, P. Rosenbusch, F. Reinhard, and J. Reichel, IEEE Trans. Ultrason. Ferroelectr. Freq. Control **57**, 88 (2010).
[49] The maser frequency is measured by the SYRTE primary standards. Its drift is at most a few 10^{-16} per day [79] and can be neglected for our purposes.
[50] W. Maineult, C. Deutsch, K. Gibble, J. Reichel, and P. Rosenbusch, Phys. Rev. Lett. **109**, 020407 (2012).
[51] C. F. Ockeloen, A. F. Tauschinsky, R. J. C. Spreeuw, and S. Whitlock, Phys. Rev. A **82**, 061606 (2010).
[52] G. Reinaudi, T. Lahaye, Z. Wang, and D. Guéry-Odelin, Opt. Lett. **32**, 3143 (2007).
[53] D. W. Allan, Proc. IEEE **54**, 221 (1966).
[54] http://www.wriley.com
[55] The minimum time of flight is given by the onset of optical diffraction at high optical density.
[56] P. Böhi, M. F. Riedel, J. Hoffrogge, J. Reichel, T. W. Hänsch, and P. Treutlein, Nature Phys. **5**, 592 (2009).
[57] L. Sárkány, P. Weiss, H. Hattermann, and J. Fortágh, Phys. Rev. A **90**, 053416 (2014).
[58] G. J. Dick, *Local Oscillator Induced Instabilities in Trapped Ion Frequency Standards*, Technical Report (DTIC, Ft. Belvoir, 1987).
[59] G. Santarelli, C. Audoin, A. Makdissi, P. Laurent, G. J. Dick, and C. Clairon, IEEE Trans. Ultrason. Ferroelectr. Freq. Control **45**, 887 (1998).
[60] The sensitivity function can be understood by visualizing the trajectory of a spin 1/2 on the Bloch sphere.
[61] A. Luiten, A. Mann, M. Costa, and D. Blair, IEEE Trans. Instrum. Meas. **44**, 132 (1995).
[62] A. G. Mann, C. Sheng, and A. N. Luiten, IEEE Trans. Instrum. Meas. **50**, 519 (2001).
[63] J. Guéna, M. Abgrall, D. Rovera, P. Laurent, B. Chupin, M. Lours, G. Santarelli, P. Rosenbusch, M. E. Tobar, R. Li *et al.*, IEEE Transactions on Ultrasonics, Ferroelectrics and Frequency Control **59**, 391 (2012).
[64] D. Chambon, S. Bize, M. Lours, F. Narbonneau, H. Marion, A. Clairon, G. Santarelli, A. Luiten, and M. Tobar, Rev. Sci. Instrum. **76**, 094704 (2005).
[65] K. Dieckmann, R. J. C. Spreeuw, M. Weidemüller, and J. T. M. Walraven, Phys. Rev. A **58**, 3891 (1998).
[66] V. Dugrain, P. Rosenbusch, and J. Reichel, Rev. Sci. Instrum. **85**, 083112 (2014).
[67] A. Bartels, S. A. Diddams, C. W. Oates, G. Wilpers, J. C. Bergquist, W. H. Oskay, and L. Hollberg, Opt. Lett. **30**, 667 (2005).
[68] J. Millo, R. Boudot, M. Lours, P. Bourgeois, A. Luiten, Y. L. Coq, Y. Kersalé, and G. Santarelli, Opt. Lett. **34**, 3707 (2009).
[69] J. Kim and F. X. Kärtner, Opt. Lett. **35**, 2022 (2010).
[70] P. DelHaye, A. Schliesser, O. Arcizet, T. Wilken, R. Holzwarth, and T. Kippenberg, Nature (London) **450**, 1214 (2007).

[71] P. Westergaard, J. Lodewyck, and P. Lemonde, IEEE Trans. Ultrason. Ferroelectr. Freq. Control **57**, 623 (2010).
[72] S. Bernon, T. Vanderbruggen, R. Kohlhaas, A. Bertoldi, A. Landragin, and P. Bouyer, New J. Phys. **13**, 065021 (2011).
[73] J. Lodewyck, P. G. Westergaard, and P. Lemonde, Phys. Rev. A **79**, 061401 (2009).
[74] M. Kohnen, P. Petrov, R. Nyman, and E. Hinds, New J. Phys. **13**, 085006 (2011).
[75] J. Esteve, T. Schumm, J.-B. Trebbia, I. Bouchoule, A. Aspect, and C. I. Westbrook, The European Physical Journal D-Atomic, Molecular, Optical and Plasma Physics **35**, 141 (2005).
[76] C. D. J. Sinclair, E. A. Curtis, I. L. Garcia, J. A. Retter, B. V. Hall, S. Eriksson, B. E. Sauer, and E. A. Hinds, Phys. Rev. A **72**, 031603(R) (2005).
[77] S. Jose, P. Surendran, Y. Wang, I. Herrera, L. Krzemien, S. Whitlock, R. McLean, A. Sidorov, and P. Hannaford, Phys. Rev. A **89**, 051602 (2014).
[78] V. Leung, D. Pijn, H. Schlatter, L. Torralbo-Campo, A. La Rooij, G. Mulder, J. Naber, M. Soudijn, A. Tauschinsky, C. Abarbanel *et al.*, Rev. Sci. Instrum. **85**, 053102 (2014).
[79] ftp://ftp2.bipm.org/pub/tai//publication/cirt/